Geophysical Research Letters

RESEARCH LETTER
10.1029/2023GL105624

Increasing Flood Hazard Posed by Tropical Cyclone Rapid Intensification in a Changing Climate

Joseph W. Lockwood[1], Ning Lin[2], Avantika Gori[2], and Michael Oppenheimer[1,3,4]

[1]Department of Geoscience, Princeton University, Princeton, NJ, USA, [2]Civil and Environmental Engineering, Princeton University, Princeton, NJ, USA, [3]Princeton School of Public and International Affairs, Princeton University, Princeton, NJ, USA, [4]High Meadows Environmental Institute, Princeton, NJ, USA

Key Points:

- Future climate warming causes large increases in the probability of rapid intensification (RI) within 24 hr of landfall
- RI events show notably higher rainfall hazard levels than non-RI events even with equivalent TC intensity
- Changes in RI events dominate future increases in 100-year rainfall and storm tide levels for most of the US coastline

Supporting Information:

Supporting Information may be found in the online version of this article.

Correspondence to:

J. W. Lockwood,
jl115@princeton.edu

Citation:

Lockwood, J. W., Lin, N., Gori, A., & Oppenheimer, M. (2024). Increasing flood hazard posed by tropical cyclone rapid intensification in a changing climate. *Geophysical Research Letters*, *51*, e2023GL105624. https://doi.org/10.1029/2023GL105624

Received 25 JULY 2023
Accepted 9 FEB 2024

Author Contributions:

Conceptualization: Joseph W. Lockwood, Ning Lin, Avantika Gori, Michael Oppenheimer
Data curation: Ning Lin, Avantika Gori, Michael Oppenheimer
Formal analysis: Joseph W. Lockwood, Ning Lin
Investigation: Joseph W. Lockwood, Ning Lin, Avantika Gori, Michael Oppenheimer
Methodology: Joseph W. Lockwood, Ning Lin, Avantika Gori, Michael Oppenheimer
Project administration: Michael Oppenheimer
Resources: Ning Lin, Avantika Gori, Michael Oppenheimer

Abstract Tropical cyclones (TCs) that undergo rapid intensification (RI) before landfall are notoriously difficult to predict and have caused tremendous damage to coastal regions in the United States. Using downscaled synthetic TCs and physics-based models for storm tide and rain, we investigate the hazards posed by TCs that rapidly intensify before landfall under both historical and future mid-emissions climate scenarios. In the downscaled synthetic data, the percentage of TCs experiencing RI is estimated to rise across a significant portion of the North Atlantic basin. Notably, future climate warming causes large increases in the probability of RI within 24 hr of landfall. Also, our analysis shows that RI events induce notably higher rainfall hazard levels than non-RI events with equivalent TC intensities. As a result, RI events dominate increases in 100-year rainfall and storm tide levels under climate change for most of the US coastline.

Plain Language Summary Tropical cyclones (TCs) that rapidly intensify (RI) before hitting land are typically hard to predict and cause immense destruction. We used synthetic TCs downscaled from global climate models and physics-based hazard models to examine the dangers posed by these RI storms in historical and future climates. The TC simulation shows that, as the climate warms, the number of TCs undergoing rapid intensification could rise substantially in the North Atlantic region. Additionally, the likelihood of rapid intensification within 24 hr of landfall significantly increases. These TCs are much riskier, particularly in terms of heavy rainfall, even when compared to equally strong TCs that did not rapidly intensify. Consequently, 100-year rainfall and storm tide levels will greatly increase under climate change, largely due to the increase of RI events in the future.

1. Introduction

Tropical cyclones (TCs) that undergo rapid intensification (RI) often become high intensity storms, which are responsible for the majority of the fatalities and damage from TCs (Emanuel, 2017). Notable examples include Hurricanes Andrew (1992) and Katrina (2004), which escalated into formidable high intensity storms, resulting in significant loss of life and extensive damages. RI is commonly measured as a substantial increase in wind intensity occurring within a brief duration. Many studies opt to define it as a change in 30 knots within a 24-hr timeframe (Kaplan & DeMaria, 2003; Lee et al., 2016), although some define it at as a change of 35 (Lu et al., 2023) or 45 knots (Li et al., 2022) within 24 hr. Over the last 30 years of the historical record in the North Atlantic, the 95th percentile of intensity changes in the North Atlantic corresponds to a change of 35 knots over 24 hr (Balaguru et al., 2018). The brief time-scales involved in RI, if it happens near landfall, present a pressing challenge, as coastal communities may have limited opportunity to initiate evacuation measures and adequately prepare for the arrival of an exceptionally intense TC, as exemplified by the historical event of Hurricane Audrey in 1957.

Forecasting RI of TCs is particularly problematic; RI events are responsible for intensity forecasts with the highest errors, and few operational models are skillful in predicting RI (DeMaria et al., 2021). The difficulty of operationally predicting RI is due in large part to the multiscale nature of the problem with environmental, oceanic, and inner-core processes all likely playing important roles in determining when a TC will undergo RI (Elsberry et al., 2021; Kaplan & DeMaria, 2003; Kaplan et al., 2015). Prior studies suggest that the occurrence of RI is primarily influenced by environmental factors (Bhatia et al., 2022; Lu et al., 2023); Kaplan and DeMaria (2003) found over the historical record in the North Atlantic that RI events form in regions with warmer SSTs and higher lower-tropospheric relative humidity compared to non-RI cases.

Software: Joseph W. Lockwood, Ning Lin, Avantika Gori
Supervision: Ning Lin, Avantika Gori, Michael Oppenheimer
Validation: Joseph W. Lockwood, Ning Lin, Avantika Gori
Visualization: Joseph W. Lockwood, Ning Lin, Avantika Gori, Michael Oppenheimer
Writing – original draft: Joseph W. Lockwood, Ning Lin, Avantika Gori, Michael Oppenheimer
Writing – review & editing: Joseph W. Lockwood, Ning Lin, Avantika Gori, Michael Oppenheimer

Historical destruction associated with TCs that undergo RI have inspired new research on whether RI frequency will increase into the future. A recent statistical-deterministic downscaling study found that the number of TCs that undergo RI before U.S. landfall is projected to significantly increase in the late 21st century compared to the late 20th century, particularly within 24 hr of making landfall (Emanuel, 2017). Using a coupled high-resolution global climate model (GCM), Bhatia et al. (2018) projected a large increase in the incidence of RI due to global warming, with large portions of every basin expected to experience a significant increase in the percentage of TCs that undergo RI. Jing et al. (2021) performed statistical and statistical-deterministic downscaling of the GCM used in Bhatia et al. (2018), and projected significant increase in RI events, although the extent of increase varies among the downscaling methods. Finally, theory of TC intensification implies that the maximum rate of intensification increases with the square of the potential intensity (Emanuel, 1987), which is expected to increase at an approximate rate of 2%–3% per 1° global mean temperature change (Knutson et al., 2020; Lockwood, Oppenheimer, et al., 2022).

Despite these expected changes in TCs that undergo RI, no studies to our knowledge have assessed the role of RI on flood hazard. In this study, we use synthetic TCs generated by the statistical-deterministic model and utilize physics-based storm tide and rain rate models to assess the hazards presented by TCs that undergo RI. Our analysis encompasses an exploration of changes in North Atlantic RI metrics from historical to mid-emissions climate scenarios, as well as an examination of the distinctions in storm tide and rain rate levels produced by RI before landfall and non-RI events. Additionally, we investigate changes in storm tide and rain rate return levels associated with changes in TCs that undergo RI before landfall compared to non-RI events along the US East and Gulf coasts.

2. Methodology

2.1. Synthetic TCs Data Sets and RI

We use 5018 synthetic TCs generated in Gori et al. (2022) for the historical period between 1980 and 2005, that are downscaled using the statistical-deterministic TC model for the National Centers for Environmental Prediction (NCEP) reanalysis (we refer to this as the historical simulation). Given the large-scale environment along the modeled track, the TC model calculates the storm intensity evolution deterministically through the use of the Coupled Hurricane Intensity Prediction System (Emanuel & Nolan, 2004). We use approximately 6000 synthetic TC generated in Xi et al. (2023), downscaled using the same TC model for years 2070–2100 of SSP2-4.5 based on six CMIP6 climate models: Canadian Earth System Model (CANESM), Centre National de Recherches Météorologiques (CNRM), EC-Earth Consortium Model (ECEARTH), Model for Interdisciplinary Research on Climate (MIROC) and UK Met Office (UKMO). Additionally, we also use TCs generated for the historical period (1980–2005) from each GCM for bias correction.

As noted in Gori et al. (2022), the downscaled TCs from each CMIP6 model may be biased compared to the NCEP-downscaled TCs, and biases within the TC characteristics can propagate to become biases in the hazard estimation. TC intensity and annual frequency are both important drivers of coastal flood risk, and both variables may be biased due to biases in CMIP6 projections. Therefore, we bias correct the frequency based on the frequency ratio between the NCEP and CMIP6 historical simulations and bias correct the intensity (Vmax) by performing the quantile delta mapping bias correction of Cannon (2018). Specifically, the change between the GCM-projected future (2070–2100) and historical (1984–2005) downscaled Vmax quantiles is added to the NCEP-downscaled historical quantiles to create a corrected future Vmax distribution for each GCM model. The deployment of modeling approaches and empirical data in this study is indicated in Figure S1 in Supporting Information S1.

Various thresholds have been utilized to define RI, with numerous studies opting to identify it based on wind speed changes such as 25, 30, and 35 knots occurring within a 24-hr timeframe or less (Bhatia et al., 2018, 2019; Lee et al., 2016). Kaplan et al. (2010) demonstrated that intensity changes of 25, 30, and 35 knots corresponded approximately to the 90th, 94th, and 97th percentiles, respectively, of 24-hr over water changes in the tropical regions of the Atlantic basins between 1989 and 2006. Over the observational record from 1986 to 2015, 35 knots or above in 24 hr is estimated to be the 95th percentile in the north Atlantic (Balaguru et al., 2018). The tracks of RI cases satisfying the 25- and 30-kt thresholds span a significant portion of the Atlantic basin, whereas cases meeting the 35-kt threshold exhibit more limited coverage, with very few instances occurring north of 30°N. Moreover, we performed a sensitivity analysis at three different threshold levels: 25, 35, and 45 knots (refer to

Figures S2–S4 in Supporting Information S1). We note that our results and conclusions are relatively insensitive to changes in the threshold. For the remainder of this paper, we choose to concentrate on the threshold of 35 knots or above in 24 hr.

Following Emanuel (2017), we separate the storms into two categories: RI events, that have rapidly intensified within the 24 hr prior to landfall, and non-rapid intensification events (non-RI), that have not rapidly intensified within 24 hr of landfall. As RI is calculated as the change over 24 hr, the calculation of RI is designed to initiate 48 hr before the time of landfall. We note that out of the 5,018 synthetic events for the historical time period, 847 undergo RI during their life cycle using a definition of 35 knots or above in 24 hr (a rate of 18%). In comparison, the IBTrACs data for the North Atlantic during the same period (1980–2005) includes 1,543 events, with 290 (or 18%) of these events undergoing RI at some point during their life cycle.

2.2. Storm Tide and Rainfall Modeling

Storm tide and rain rate estimates for the synthetic TCs are from Gori et al. (2022) and Xi et al. (2023), generated using the full physics 2D depth-integrated version of the hydrodynamic model ADvanced CIRCulation (ADCIRC; Luettich et al. (1992); Westerink et al. (1994)) and the physics-based tropical cyclone rain model (TCRM) described in Zhu et al. (2013) and Lu et al. (2018). The storm surge levels for each synthetic TC are modeled using an unstructured computational mesh developed and validated by Marsooli and Lin (2018) that spans the entire North Atlantic basin. For each event, the maximum rain rate and storm tide level is extracted at 300 sites located along the US East and Gulf Coasts.

TCRM has been evaluated against a weather and research forecasting model WRF (Lu et al., 2018) and observational data in the North Atlantic (Xi & Lin, 2022). The model has been used for TC rainfall risk assessment (Emanuel, 2017; Gori et al., 2022). TCRM is a horizontally distributed and vertically integrated numerical model, where the rain rate is related to the upward vapor flux, which is contributed by frictional convergence (Ekman pumping), changes in the axisymmetric vorticity of the gradient wind (vortex spinup and spindown), and interaction of the storm with topography and large-scale baroclinity (wind shear) (see Lu et al. (2018) for model derivation). In particular, the effect of vortex stretching (i.e., changes in the storm's vorticity), derived from the principles of mass continuity and conservation of angular momentum, depends on the time derivative of storm intensity. Thus, everything else being equal, storm intensification induces increases in rain rates.

Both the storm tide and rainfall modeling are driven primarily by the surface wind field. We represent the wind field of each synthetic TC using the physically derived complete wind profile of Chavas et al. (2015) (C15) combined with the wind intensity (maximum wind speed, Vmax) from the deterministic intensity component of the statistical-deterministic TC model and TC size information. To our knowledge, no physical model of TC outer size exists, due to a lack of physical understanding of the variation of TC outer size (Schenkel et al., 2018). Thus, to be consistent, we follow the approach of the statistical-deterministic TC model to randomly draw an outer size value based on the historical distribution of North Atlantic outer size (Chavas et al., 2016) for each synthetic TC. Then the complete wind model uses the outer size and Vmax to estimate the inner size (radius of maximum wind; Rmax) and thus the symmetrical wind field.

The Rmax estimated with this wind model is statistically consistent with the observation (Chavas et al., 2016). Using this approach, the sizes for RI and non-RI storms are from the same underlying distribution (i.e. historical outer size distribution) and, given the outer size, Rmax is inversly correlated with Vmax. The other intensity measure obtained from the TC model, pressure deficit, is also correlated to Vmax. Given the outer size, therefore, we can focus on comparing RI and non RI events with similar wind intensity (i.e., we do not need to normalize for size or pressure in our analysis).

To capture asymmetrical wind forcing, we add an empirically estimated surface background wind vector onto the symmetric wind profile (Lin & Chavas, 2012). The C15 model with the background-wind correction has been shown to capture historical rainfall and storm surges well and can reproduce the observed hazard with lower errors than the often-used Holland wind model (Holland, 1980) coupled with the translation-speed-based asymmetry (Wang et al., 2022; Xi & Lin, 2020).

Statistical analysis is performed on the modeled peak storm tides and peak rain rates to produce return level curves. Assuming that the storms arrive as a stationary Poisson process under a given climate, the return period (T_h) can be calculated as (Lin et al., 2012):

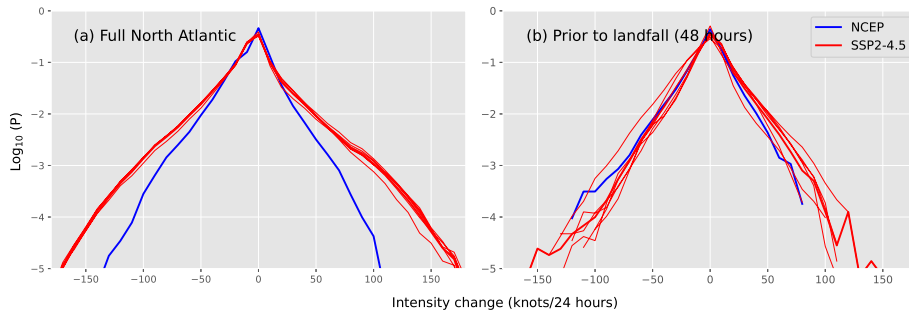

Figure 1. Common logarithm of the probability densities of 24-hr intensity change calculated from NCEP synthetic events (blue) and SSP2-4.5 (red), for the full North Atlantic basin (a) and for storms 24 hr prior to landfall (b). Thin curves show the range of six CMIP6 estimates. The average value of the CMIP6 models is calculated as the average of the six CMIP6 estimates of each intensity change level.

$$T(h) = \frac{1}{P\{H^a > h\}} = \frac{1}{1 - P\{Ha \le h\}} = \frac{1}{1 - e^{-\lambda P\{H > h\}}} \approx \frac{1}{\lambda(1 - P\{H \le h\})} \tag{1}$$

where $P(H^a \le h)$ is the cumulative density function (CDF) of the annual maximum hazard level, $P(\{H \le h)$ is the CDF of the event peak hazard level, and λ is the storm annual frequency for the location.

To assess the change in the hazard levels attributable to changes in RI, we consider the hazards generated from RI and non-RI events separately. We assume RI TCs and non-RI TCs occur as separate, independent Poisson processes with their respective arrival rates determined by the proportion of RI and non-RI landfalls at the given location. The overall hazard return period can be calculated by combining the individual RI and non-RI return periods as follows:

$$\begin{aligned} 1 - \frac{1}{T(h)} &= P\{H^a \le h\} = P\{H^a_{RI} \le h\} \cdot P\{H^a_{NRI} \le h\} = \left(1 - \frac{1}{T_{RI}(h)}\right) \cdot \left(1 - \frac{1}{T_{NRI}(h)}\right) \\ &\approx (1 - \lambda_{RI} \cdot (1 - P\{H_{RI} \le h\})) \cdot (1 - \lambda_{NRI} \cdot (1 - P\{H_{NRI} \le h\})) \end{aligned} \tag{2}$$

where $T_{(RI)}$ ($T_{(NRI)}$) is the hazard return period calculated for solely RI (non-RI) TCs, λ_{RI} (λ_{NRI}) is the yearly frequency of RI (non-RI) TCs, and $P(H_{RI} \le$ h) and $P(H_{NRI} \le h)$ are the hazard CDFs for RI and non-RI TCs, respectively.

The location-specific arrival rate is an adjustment of the basin arrival rate according to the proportion of storms passing within 200 km of each location and according to whether storms are RI or non-RI. Here, we model the tail of the hazard CDF using the Peaks-Over-Threshold method with a Generalized Pareto Distribution and maximum likelihood estimation (Coles, 2001). Non-parametric density estimations are used to model the rest of the distribution. We determine the tail threshold value by trial and error so that the smallest error in the distribution fitted to the tail is obtained.

3. Results

3.1. Future Changes in TC Intensification

Figure 1 shows the common logarithm of the probability densities of the 24-hr intensification rates calculated for the NCEP and SSP2-4.5 synthetic TCs. The data on either side of zero intensity change tend to fall on straight lines, indicating that the probability densities are nearly exponentially distributed. The 2070–2100 synthetic TCs have significantly more 24-hr intensity changes above 40 kt than the 1980–2005 NCEP TCs. The 1980–2005 NCEP simulation has zero 24-hr intensification events of 125 kt or more, but by the end of century the CMIP6 models used here indicate an increase in events exceeding 125 knots in 24 hr toward the end of the century (Figure 1b). While such a rate of intensification is nowhere apparent in the historical record and the future probability of occurrence (10^{-4}–10^{-5}) is rather low (Figure 1) the mere possibility of such rapid intensification is worthy of attention by risk managers.

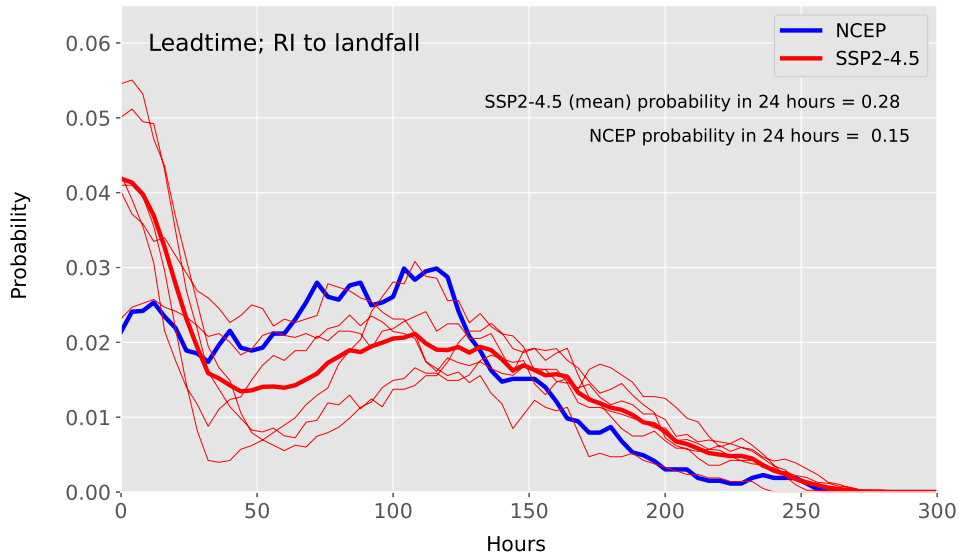

Figure 2. Probability of leadtime (hours) between onset of rapid intensification (defined as a change of at least 35 knots/24 hr) and landfall for the NCEP (blue line; 984–2005) and SSP2-4.5 simulations (red lines; 2070–2100). The thick solid red line shows the CMIP6 model mean.

We calculate the change in lead time, defined as the amount of time in hours from when a TC undergoes RI to landfall (Figure 2). For the NCEP storms, the probability of RI is relatively uniform from the time of landfall up to 120 hr before landfall. For the SSP2-4.5 emissions storms, the probability of RI happening close to landfall increases in all CMIP6 models, such that the probability of RI within 24 hr of landfall increases from 0.15 to 0.28.

We proceed to investigate the RI ratio as the count of 24-hr intensity changes that surpass 35 knots, divided by the overall number of 24-hr intensity changes at a given location. It's noted that this represents a revised version of the RI ratio, defined for 30-knot increases over 24 hr in Bhatia et al. (2018). Figure 3a shows the RI ratio for the NCEP storms, with most regions having a ratio of between 0.05 and 0.07. The highest RI ratios are in the Gulf of Mexico basin and low latitude states along the eastern coast of the US. The large RI ratio in low latitude regions shows some agreement to the location of historical events in IBTrACS that have undergone RI over the same time period (black dots on Figure 3a). The model results are also in close agreement with Bhatia et al. (2023), who found using a threshold of 30 knots over 24 hr in the historical record a RI ratio of between 0.05 and 0.1 between 1982 and 2017 across the North Atlantic basin.

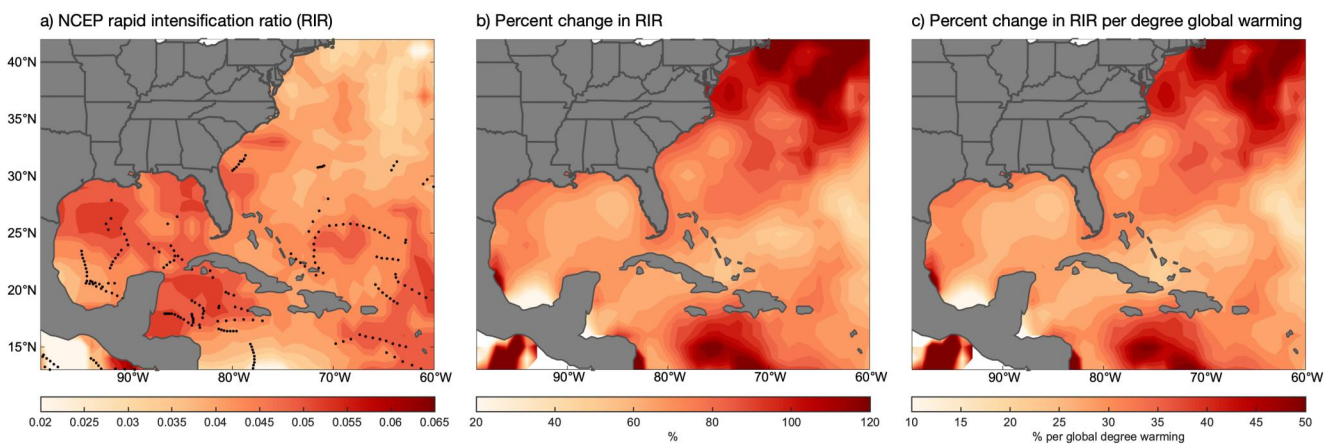

Figure 3. Maps of (a) NCEP rapid intensification ratio (RIR), (b) percentage change in RIR and (c) change in RIR per degree global warming. Change is calculated as the difference between the NCEP period and bias corrected SSP2-4.5 period. Dots on (a) show the location of RI in historical events identified in the International Best Track Archive for Climate Stewardship (IBTrACS) product for the same time period (1980–2005). Rapid intensification ratio is calculated as the number of events that rapidly intensify out of all intensity changes at each location.

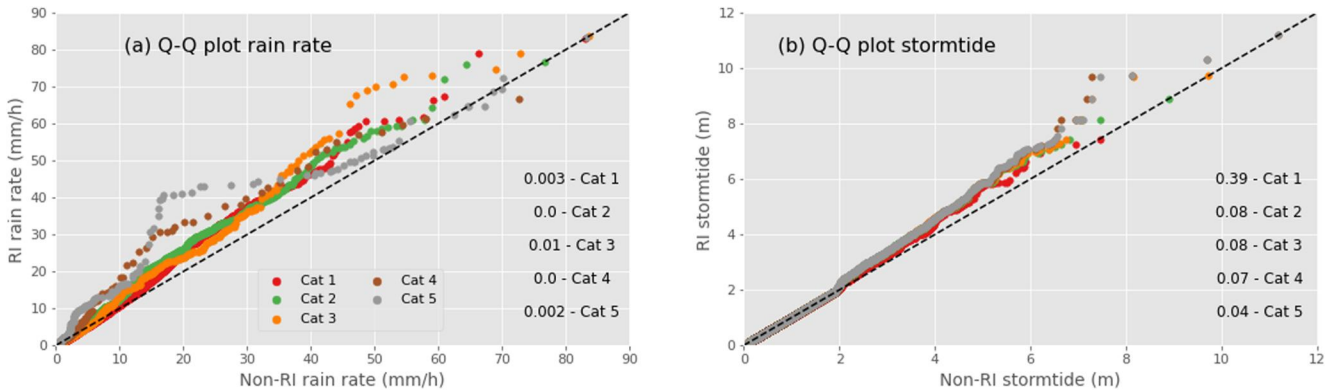

Figure 4. Q-Q plot of rain rate and storm tide levels for RI (*y*-axis) and non-RI (*x*-axis) events. RI and non-RI events are defined based on intensity change within 24 hr of landfall. The analysis is for the NCEP synthetic TCs, separated by mean storm category in the 24 hr prior to landfall. P-values for the Kolmogorov-Smirnov test of each category storm are found at lower right of both panels; if the *p*-value is below 0.05, then the non-RI and RI distributions are statistically different.

Figure 3b shows the percentage change in RI ratio from the NCEP period to the SSP2-4.5 future period (averaged over the CMIP6 models). We find strong increases in RI ratio by the end of the twenty first century, with many regions projected to have a 30%–100% increase. Importantly, the majority of the TC-prone coastal regions show a significantly higher increase in RI ratio compared to the open ocean regions. There are particularly large increases along the Western Gulf of Mexico and along mid to high latitude Atlantic region. Figure 3c shows the percentage increase in RI ratio per degree global warming, calculated for each CMIP6 model individually before being averaged across the models. The percentage of TCs reaching or surpassing a 35 knots/24 hr intensity threshold is projected to rise by 10%–30% for each degree of global mean temperature increase by the century's end. Some high latitude regions are projected to have an increase in RIR by up to 50% or greater per degree temperature change in the future, as these regions are characterized by historically low RI ratio and thus even a minor increase in RI events would signify a substantial percentage change.

3.2. Flood Hazard Associated With RI Events

We next explore if the flood hazards generated by RI events are statistically different from non-RI events. To do this we use quantile–quantile maps (QQplot) to examine the distribution of storm tide levels and rain rate values modeled for the NCEP storms for each intensity category (Figure 4). Specifically, Figure 4 shows the quantiles of rain rates and storm tide levels at 300 locations along the US East and Gulf Coasts for RI versus non-RI storms. The QQplot determines if two data sets come from populations with a common distribution; if the estimates fall on the dotted line then they are likely from the same distribution. Also, we separate the storms into the average wind-speed intensity categories (1–5) in the 24 hr before landfall.

We find that the rain rates produced by RI events are larger when compared to non-RI events, with the same intensity category (Figure 4a). To test whether the hazard produced by each category of storms is statistically different, we use the two sided Kolmogorov-Smirnov test. We find that there are significant difference in rain rate for all categories at 95% significance level (p-value below 0.05), and thus they are likely from different distributions.

Storm tide levels produced by category 5 RI TCs are also significantly higher than non-RI TCs of the same magnitude, with a p-value below 0.05 (Figure 4b), but the difference is not significant for other categories. Thus, storm tide is relatively less sensitive to RI compared to rain rate levels, except for the strongest storms. This may be a result of the rain rates levels being more directly influenced by changes in storm intensity change, as in the TCRM. Additionally, storm surge is also significantly influenced by other factors unrelated to intensity, including the shape of the coastline, depth of the continental shelf and storm translation speed (Lockwood, Lin, et al., 2022).

Finally, the large increases in probability of RI into the future may suggest an increase in TCs that rapidly intensify in short time-scales close to landfall. To explore the change in hazard, we focus here on the change in 100 years return level at the 300 sites along the US East and Gulf coasts. For all locations, there is considerable increases in the 100 years return level for both rain rates and storm tides into the future period (green lines

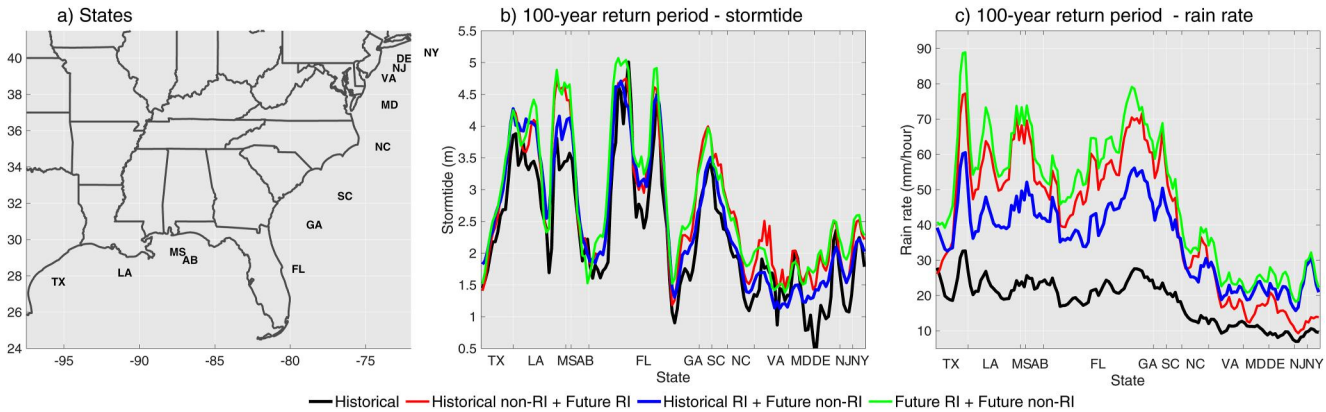

Figure 5. Projected changes to the 100-year hazard level for (b) storm tide levels and (c) rain rate at (a) locations along the East and Gulf Coasts. The black line is all NCEP storms; the red line shows the historical non-RI events combined with SSP2-4.5 RI events; and the blue line shows the historical RI events combined with SSP2-4.5 non-RI events. The green lines show the combined change in RI and non-RI. RI and non-RI events are defined based on intensity change within 24 hr of landfall.

showing total change on Figure 5). Our projections show that TC changes have a relatively small impact on the 100 years return level at high latitudes, whereas its impact at lower latitudes is as high as 1.5 m for storm tides and 30 mm/hr for rain rates.

To explore the importance of RI changes on future hazards we calculate the change in 100-year return levels for storm tides and rain rates isolating the change attributed to the changes in RI and non-RI events separately (Figure 5). At the majority of locations in the Gulf of Mexico and South East Atlantic, effects of RI storm changes on the 100 years hazard levels are considerably larger than effects of non-RI storm changes, especially for rainfall hazards (Figure 5). It is plausible that the reduction of the relative importance of RI events on 100 years return levels with latitude is related to the relatively low frequency of these events even in future climate scenarios at higher latitudes.

4. Discussion and Conclusions

Theory of TC intensification implies that the maximum rate of intensification increases with the square of the potential intensity (Emanuel, 1987), the latter is expected to increase with an approximate rate of 2%–3% per 1° (Knutson et al., 2020; Lockwood, Oppenheimer, et al., 2022). Indeed, we find that the proportion of TCs that rapidly intensify increases substantially into the future across Atlantic basin and particularly near the US East and Gulf Coasts. As a result, the probability of RI within 24 hr of landfall increases substantially under SSP2-4.5. These results suggest that coastal communities will have less time to prepare and evacuate from the onset of RI to landfall into the future.

Jing et al. (2021) conducted both statistical and statistical-deterministic downscaling of the Geophysical Fluid Dynamics Laboratory's High-Resolution Forecast-Oriented Low Ocean Resolution (HiFLOR) model under the representative concentration pathway 4.5 (RCP4.5). They found that the extent of increase in RI events varies among the downscaling methods, suggesting that our results may differ under different TC downscaling models. Under the RCP4.5 scenario, HiFLOR demonstrated a significant rise in RI ratio, using a definition as storms with a velocity increase of 30 knots over 24 hr, reaching a staggering 76% increase by the period 2081–2100. In comparison, the statistical-deterministic model (Emanuel et al., 2006) and the Princeton environment-dependent probabilistic tropical cyclone (PepC; Jing & Lin, 2020) downscaling methods exhibited notable increases of 20.5% and 10.8%, respectively, under the same scenario (Jing et al., 2021). Our findings align with these outcomes, revealing similar trends for the years 2070–2100. We employ a more conservative definition of RI, necessitating an increase of 35 knots or greater within a 24-hr period, and project increases of RI ratio ranging from 30% to 70% for the SSP2-4.5 scenario based on the CMIP6 models used here.

Instead of using high-resolution GCMs, which are mainly employed to study changes in average RI rates, we opted for a statistical-deterministic downscaling approach. Given available computational resources, this method enables us to model the hazards for a very large set of TCs to investigate the impact of RI events on extreme hazards with a long return period such as 100 years. Further research could use different approaches, that avoid

the underlying assumptions made in the statistical-deterministic framework, to study RI impact on coastal hazards. We acknowledge the potential benefits of utilizing ensembles of high-resolution GCM simulations for this purpose, but presently, such an approach would be excessively costly.

We find that there are statistical differences in the rain rates produced by RI events when compared to non-RI events for storms of the same intensity, due to the physically derived stretching mechanism that influences rain rates in the TCRM model. Specifically, storm intensification, which is associated with an inward shift of angular momentum surfaces (increasing maximum wind intensity and decreasing radius of maximum wind), leads to positive vertical velocity (air lifting, more rainfall) within the core and inner radius. This vortex-stretching effect varies greatly with storm intensity evolution, with the vortex-stretching-induced increase in the vertical velocity in TCRM being a function of the radial and time derivatives of the angular momentum/azimuthal wind (Lu et al., 2018). Thus, the large changes in wind and radius of maximum wind that occur during RI will result in higher vertical velocity and rainfall rates compared to non-RI events with the same intensity.

Larger rainfall hazards in RI storms compared to non-RI storms have been observed in historical events, although most of previous studies didn't control for intensity. Multiple studies, including Rogers et al. (2013); Jiang et al. (2011), have shown that the inner-core convection in TCs undergoing RI tends to be more robust than that observed in non-RI TCs. Specifically, research using composites of airborne Doppler observations from NOAA P-3 aircraft missions, as conducted by Rogers et al. (2013), revealed greater azimuthal coverage of eyewall and outer-core precipitation in RI TCs. Moreover, a comprehensive study utilizing a decade of Tropical Rainfall Measuring Mission data by Jiang et al. (2011) uncovered statistically significant disparities in convective intensity parameters within the inner core between RI and non-RI storms. The findings from Jiang et al. (2011) further demonstrated that RI storms consistently exhibit a larger rain fall area and greater total volumetric rainfall in the inner core, thus substantiating the expectation of larger rain rates during RI events. Larger rain rates for RI events has also been observed due to the rapid reorganization of the cyclone's mesoscale cloud and rain structures when a TC undergoes RI (Houze, 2010).

We did not find a significant difference in storm tide between RI and non-RI storms with the same intensity, except for category 5 TCs. This lack of identified difference indicates that the effect of RI on storm tide is small compared to the effects of storm intensity, geophysical location, and astronomical tide. We note that in this modeling set-up with the outer size of the TCs derived from an empirical lognormal distribution (Chavas et al., 2015), wind intensity has an inverse correlation with Rmax. However, storm track including storm forward speed, can affect also storm surge levels, but its effect are complex depending on coastal geometry (Lockwood, Lin, et al., 2022). We have not examined if the track features of RI storms are different from those of non-RI storms. Future research should more thoroughly explore the impact of RI on storm surge levels.

Several studies indicate a substantial projected rise in rainfall and storm surge levels along the US East and Gulf Coasts into the future (Guzman & Jiang, 2021; Wing et al., 2022). In alignment with these findings, we compare the change in 100 years rain rate and storm tide hazard levels for RI and non-RI events at locations along the US East and Gulf Coasts. Our analysis reveals that the increases in flood hazard related to increases in RI events are notably more pronounced than those associated with changes in non-RI events, particularly concerning rainfall hazards.

Our results suggest that coastal communities, particularly in low latitude regions will not only need to adapt to higher rainfall rates and storm tide levels, but also to TCs that rapidly intensify in short time-scales close to land. This may lead to disastrous scenarios when coastal areas are not given adequate notice to evacuate and prepare. This, together with increasing sea levels, implies the need for enhanced focus on refining hurricane intensity forecasts and preparing communities to quickly react to high-intensity hurricanes making landfall.

Data Availability Statement

You can access the hurricane data set IBTrACS from the National Climatic Data Center Knapp et al. (2010). The original synthetic TC data sets used in this study are available for research purposes and can be obtained freely from Kerry Emanuel. For detailed information about the synthetic data sets and their availability, please refer to Emanuel (2021).

Acknowledgments
This study was supported by the U.S. National Science Foundation Grants 1854993 and 2103754 as part of the Megalopolitan Coastal Transformation Hub.

References

Balaguru, K., Foltz, G. R., & Leung, L. R. (2018). Increasing magnitude of hurricane rapid intensification in the central and eastern tropical Atlantic. *Geophysical Research Letters*, *45*(9), 4238–4247. https://doi.org/10.1029/2018GL077597

Bhatia, K., Baker, A., Yang, W., Vecchi, G., Knutson, T., Murakami, H., et al. (2022). Tropical cyclone rapid intensification: An explanation for the global increase. https://doi.org/10.21203/rs.3.rs-1617224/v1

Bhatia, K., Baker, A., Yang, W., Vecchi, G., Knutson, T., Murakami, H., et al. (2023). Author correction: A potential explanation for the global increase in tropical cyclone rapid intensification. *Nature Communications*, *14*(1), 521. https://doi.org/10.1038/s41467-023-36308-3

Bhatia, K., Vecchi, G., Knutson, T., Murakami, H., Kossin, J., Dixon, K., & Whitlock, C. (2019). Recent increases in tropical cyclone intensification rates. *Nature Communications*, *10*(1), 635. https://doi.org/10.1038/s41467-019-08471-z

Bhatia, K., Vecchi, G., Murakami, H., Underwood, S., & Kossin, J. (2018). Projected response of tropical cyclone intensity and intensification in a global climate model. *Journal of Climate*, *31*(20), 8281–8303. https://doi.org/10.1175/JCLI-D-17-0898.1

Cannon, A. (2018). Multivariate quantile mapping bias correction: An n-dimensional probability density function transform for climate model simulations of multiple variables. *Climate Dynamics*, *50*(1–2), 31–49. https://doi.org/10.1007/s00382-017-3580-6

Chavas, D., Lin, N., & Emanuel, K. (2015). A model for the complete radial structure of the tropical cyclone wind field. Part I: Comparison with observed structure. *Journal of the Atmospheric Sciences*, *72*(9), 3647–3662. https://doi.org/10.1175/JAS-D-15-0014.1

Chavas, D., Lin, N., & Emanuel, K. (2016). A model for the complete radial structure of the tropical cyclone wind field. Part II: Wind field variability. *Journal of the Atmospheric Sciences*, *72*(9), 3647–3662. https://doi.org/10.1175/JAS-D-15-0185.1

Coles, S. (2001). An introduction to statistical modeling of extreme values.

DeMaria, M., Franklin, J. L., Onderlinde, M. J., & Kaplan, J. (2021). Operational forecasting of tropical cyclone rapid intensification at the National Hurricane Center. *Atmosphere*, *12*(6), 683. https://doi.org/10.3390/atmos12060683

Elsberry, R. L., Tsai, H.-C., Chin, W.-C., & Marchok, T. P. (2021). Predicting rapid intensification events following tropical cyclone formation in the western North Pacific based on ECMWF ensemble warm core evolutions. *Atmosphere*, *12*(7), 847. https://doi.org/10.3390/atmos12070847

Emanuel, K. (1987). Intensity on climate (Vol. *1–3*).

Emanuel, K. (2017). Will global warming make hurricane forecasting more difficult? *Bulletin of the American Meteorological Society*, *98*(3), 495–501. https://doi.org/10.1175/BAMS-D-16-0134.1

Emanuel, K. (2021). Response of global tropical cyclone activity to increasing CO_2: Results from downscaling CMIP6 models. *Journal of Climate*, *34*(1), 57–70. https://doi.org/10.1175/JCLI-D-20-0367.1

Emanuel, K., & Nolan, D. S. (2004). Tropical cyclone activity and the global climate system. *26th conference on hurricanes and tropical meteorology* (pp. 240–241).

Emanuel, K., Ravela, S., Vivant, E., & Risi, C. (2006). A statistical deterministic approach to hurricane risk assessment. *Bulletin of the American Meteorological Society*, *87*(3), 299–314. https://doi.org/10.1175/BAMS-87-3-299

Gori, A., Lin, N., Xi, D., & Emanuel, K. (2022). Tropical cyclone climatology change greatly exacerbates us extreme rainfall–surge hazard. *Nature Climate Change*, *12*(2), 1–8. https://doi.org/10.1038/s41558-021-01272-7

Guzman, O., & Jiang, H. (2021). Global increase in tropical cyclone rain rate. *Nature Communications*, *12*(1), 5344. https://doi.org/10.1038/s41467-021-25685-2

Holland, G. J. (1980). An analytic model of the wind and pressure profiles in hurricanes. *Monthly Weather Review*, *108*(8), 1212–1218. https://doi.org/10.1175/1520-0493(1980)108⟨1212:AAMOTW⟩2.0.CO;2

Houze, R. (2010). Clouds in tropical cyclones. *Monthly Weather Review*, *138*(2), 293–344. https://doi.org/10.1175/2009MWR2989a.1

Jiang, H., Liu, C., & Zipser, E. J. (2011). A trmm-based tropical cyclone cloud and precipitation feature database. *Journal of Applied Meteorology and Climatology*, *50*(6), 1255–1274. https://doi.org/10.1175/2011JAMC2662.1

Jing, R., & Lin, N. (2020). An environment-dependent probabilistic tropical cyclone model. *Journal of Advances in Modeling Earth Systems*, *12*(3), e2019MS001975. https://doi.org/10.1029/2019MS001975

Jing, R., Lin, N., Emanuel, K., Vecchi, G., & Knutson, T. R. (2021). A comparison of tropical cyclone projections in a high-resolution global climate model and from downscaling by statistical and statistical-deterministic methods. *Journal of Climate*, *34*(23), 9349–9364. https://doi.org/10.1175/JCLI-D-21-0071.1

Kaplan, J., & DeMaria, M. (2003). Large-scale characteristics of rapidly intensifying tropical cyclones in the North Atlantic basin. *Weather and Forecasting*, *18*(6), 1093–1108. https://doi.org/10.1175/1520-0434(2003)018⟨1093:LCORIT⟩2.0.CO;2

Kaplan, J., DeMaria, M., & Knaff, J. A. (2010). A revised tropical cyclone rapid intensification index for the Atlantic and eastern North Pacific basins. *Weather and Forecasting*, *25*(1), 220–241. https://doi.org/10.1175/2009WAF2222280.1

Kaplan, J., Rozoff, C. M., DeMaria, M., Sampson, C. R., Kossin, J. P., Velden, C. S., et al. (2015). Evaluating environmental impacts on tropical cyclone rapid intensification predictability utilizing statistical models. *Weather and Forecasting*, *30*(5), 1374–1396. https://doi.org/10.1175/WAF-D-15-0032.1

Knapp, K. R., Kruk, M. C., Levinson, D. H., Diamond, H. J., & Neumann, C. J. (2010). The international best track archive for climate stewardship (IBTrACS): Unifying tropical cyclone data [Dataset]. Bulletin of the American Meteorological Society, *91*, 363–376. https://doi.org/10.1175/2009BAMS2755.1

Knutson, T., Camargo, S. J., Chan, J. C. L., Emanuel, K., Ho, C.-H., Kossin, J., et al. (2020). Tropical cyclones and climate change assessment: Part II: Projected response to anthropogenic warming. *Bulletin of the American Meteorological Society*, *101*(3), E303–E322. https://doi.org/10.1175/BAMS-D-18-0194.1

Lee, C., Tippett, M., Sobel, A., & Camargo, S. (2016). Rapid intensification and the bimodal distribution of tropical cyclone intensity. *Nature Communications*, *7*(1), 10625. https://doi.org/10.1038/ncomms10625

Li, Y., Tang, Y., Toumi, R., & Wang, S. (2022). Revisiting the definition of rapid intensification of tropical cyclones by clustering the initial intensity and inner-core size. *Journal of Geophysical Research: Atmospheres*, *127*(20), e2022JD036870. https://doi.org/10.1029/2022JD036870

Lin, N., & Chavas, D. (2012). On hurricane parametric wind and applications in storm surge modeling. *Journal of Geophysical Research*, *117*(D9), D09120. https://doi.org/10.1029/2011JD017126

Lin, N., Emanuel, K., Oppenheimer, M., & Vanmarcke, E. (2012). Physically based assessment of hurricane surge threat under climate change. *Nature Climate Change*, *2*(6), 462–467. https://doi.org/10.1038/nclimate1389

Lockwood, J., Lin, N., Oppenheimer, M., & Lai, C.-Y. (2022). Using neural networks to predict hurricane storm surge and to assess the sensitivity of surge to storm characteristics. *Journal of Geophysical Research: Atmospheres*, *127*(24), e2022JD037617. https://doi.org/10.1029/2022JD037617

Lockwood, J., Oppenheimer, M., Lin, N., Kopp, R. E., Vecchi, G. A., & Gori, A. (2022). Correlation between sea-level rise and aspects of future tropical cyclone activity in CMIP6 models. *Earth's Future*, *10*(4), e2021EF002462. https://doi.org/10.1029/2021EF002462

Lu, D., Ding, R., Zhong, Q., Mao, J., Zou, Q., & Li, J. (2023). A rapid intensification warning index for tropical cyclones based on the analog method. *Geophysical Research Letters*, *50*(4), e2022GL101951. https://doi.org/10.1029/2022GL101951

Lu, P., Lin, N., Emanuel, K., Chavas, D., & Smith, J. (2018). Assessing hurricane rainfall mechanisms using a physics-based model: Hurricanes Isabel (2003) and Irene (2011). *Journal of the Atmospheric Sciences*, *75*(7), 2337–2358. https://doi.org/10.1175/JAS-D-17-0264.1

Luettich, R., Jr., Westerink, J., & Scheffner, N. (1992). Adcirc: An advanced three-dimensional circulation model for shelves, coasts, and estuaries. Report 1. Theory and methodology of adcirc-2ddi and adcirc-3dl. Dredging Research Program Tech. Rep. DRP-92-6 (p. 143).

Marsooli, R., & Lin, N. (2018). Numerical modeling of historical storm tides and waves and their interactions along the U.S. East and Gulf Coasts. *Journal of Geophysical Research: Oceans*, *123*(5), 3844–3874. https://doi.org/10.1029/2017JC013434

Rogers, R., Reasor, P., & Lorsolo, S. (2013). Airborne Doppler observations of the inner-core structural differences between intensifying and steady-state tropical cyclones. *Monthly Weather Review*, *141*(9), 2970–2991. https://doi.org/10.1175/MWR-D-12-00357.1

Schenkel, B. A., Lin, N., Chavas, D., Vecchi, G. A., Oppenheimer, M., & Brammer, A. (2018). Lifetime evolution of outer tropical cyclone size and structure as diagnosed from reanalysis and climate model data. *Journal of Climate*, *31*(19), 7985–8004. https://doi.org/10.1175/JCLI-D-17-0630.1

Wang, S., Lin, N., & Gori, A. (2022). Investigation of tropical cyclone wind models with application to storm tide simulations. *Journal of Geophysical Research: Atmospheres*, *127*(17), e2021JD036359. https://doi.org/10.1029/2021JD036359

Westerink, J., Luettich, R., Jr., Blain, C., & Scheffner, N. (1994). Adcirc: An advanced three-dimensional circulation model for shelves, coasts, and estuaries. Report 2. User's manual for adcirc-2ddi (p. 168).

Wing, O. E. J., Lehman, W., Bates, P. D., Sampson, C. C., Quinn, N., Smith, A. M., et al. (2022). Inequitable patterns of US flood risk in the Anthropocene. *Nature Climate Change*, *12*(2), 156–162. https://doi.org/10.1038/s41558-021-01265-

Xi, D., & Lin, N. (2022). Understanding uncertainties in tropical cyclone rainfall hazard modeling using synthetic storms. *Journal of Hydrometeorology*, *23*(6), 925–946. https://doi.org/10.1175/JHM-D-21-0208.1

Xi, D., Lin, N., & Gori, A. (2023). Increasing sequential tropical cyclone hazards along the US east and gulf coasts. *Nature Climate Change*, *13*(3), 1–8. https://doi.org/10.1038/s41558-023-01595-7

Xi, D., Lin, N., & Smith, J. (2020). Evaluation of a physics-based tropical cyclone rainfall model for risk assessment. *Journal of Hydrometeorology*, *21*(9), 1–59. https://doi.org/10.1175/JHM-D-20-0035.1

Zhu, L., Quiring, S. M., & Emanuel, K. A. (2013). Estimating tropical cyclone precipitation risk in Texas. *Geophysical Research Letters*, *40*(23), 6225–6230. https://doi.org/10.1002/2013GL058284